Int. J. Electrochem. Sci., 17 **(2022)** Article Number: 22064, doi: 10.20964/2022.06.29

International Journal of
ELECTROCHEMICAL
SCIENCE
www.electrochemsci.org

Short Communication

Preparation and Characterization of 3D Porous Silicon Anode Material for Lithium-Ion Battery Application

Nacer Badi[1,2,3,*], *Azemtsop Manfo Theodore*[4,*], *Aashis Roy*[5], *Saleh A. Alghamdi*[1,2,3], *Ahmed Obaid M Alzahrani*[6,7], *Alex Ignatiev*[8]

[1] Renewable Energy Laboratory, Department of Physics, Faculty of Science, University of Tabuk, Tabuk 71491, Kingdom of Saudi Arabia
[2] Nanotechnology Research Unit, University of Tabuk, Tabuk 71491, Kingdom of Saudi Arabia
[3] Renewable Energy & Energy Efficiency Center, University of Tabuk, Tabuk 71491, Kingdom of Saudi Arabia
[4] Center of Excellence on Solar Cells & Renewable Energy, School of Basic Science and Research, Sharda University, Greater Noida- 201310, India
[5] Department of Chemistry, S.S.Tegnoor Degree College, Gubbi Colony -585105, Kalaburagi, Karnataka India
[6] Physics Department, Faculty of Science, King Abdulaziz University, Jeddah, Saudi Arabia
[7] Center of Nanotechnology, King Abdulaziz University, Jeddah, Saudi Arabia
[8] Department of Physics, University of Houston, Houston, TX77204-5004, USA
[*]E-mail: nbadi@ut.edu.sa, azemsouleymane@yahoo.fr

Received: 3 January 2021 / *Accepted:* 28 March 2022 / *Published:* 7 May 2022

Three-dimensional (3D) Si materials with interconnected pores have been synthesized and used applied in lithium-ion batteries (LIBs) as anode material via a conventional method of sputtering, thermal evaporation. The result was found to be satisfactory regarding the device performance. In this work, porous Si materials have been prepared as active material using silicon powder and proppant and characterized using scanning electron microscopy (SEM), x-ray diffraction (XRD) and Raman spectroscopy techniques. 3D porous Si products coated onto Cu current collector led to enhanced surface area and energy density in LIB. The performance of LIB cells is evaluated via electrochemical characterization. The 3D porous Si materials in LIB exhibited better capacitance and cyclic performance than Si powder anode. The battery offers a discharge capacity of 267.1 mAh g^{-1} at 298 mA g^{-1} with a capacity retention of 95.5% after 50 cycles and the battery capacity remains stable between 40-50 cycles.

Keywords: lithium-ion battery, porous silicon, energy density, coulombic efficiency

1. INTRODUCTION

In our today's society, LIBs have dominated the market of advanced energy sources, since they are widely applied in many sectors such as electronics, electric vehicles, and energy storage systems. Particular attention has been given to Si because it can coordinate with $4.4Li^+$ ($Li_{4.4}Si$) per atom, exhibiting a capacity of 4200 mAh g^{-1} greater than that delivered with traditional graphite materials. With the aim of ameliorating the capacity and cycle life of silicon anodes, scientists studied the insertion of a particle in a matrix including Li-ion/electron transfer [1-13]. This is a promising method to improve mechanical stability. Silicon commercialized are accessible in aggregated microparticles with an average size of 30 nm. Therefore, minimizing the size is decisive and each particle should be covered by Li^+-ions, leading to the active phase that stops the particle accumulation while operating [14-18]. In contrast, when nanowires are distantly separated and the regular pores acting as barrier contributes to invariable volume transitions. As an example, mesoporous SnO_2 developed by solid or soft model [19-22] exhibited a very good capacity of retention better than nanosized duplicate indicating the impact of mesoporous structures. Silicon (Si) as anode material is employed in LIBs because of its good theoretical capacity and sufficient resources [23-25]. Using porous structured Si as anode material presents many advantages for LIB such as reducing the volume variation when Li^+ ions are inserted or extracted, reducing the Li^+ transfer track, offering enough contact, and ameliorating the ion transport at the electrode/electrolyte interface [26-31]. Porous Si materials can be produced using chemical etching approaches, such as wet chemical/electrochemical etching, and metal-assisted chemical etching [32]. Nevertheless, a generation of 30-40% of porous Si can be produced via the chemical etching path as well as template procedure. 3D structurally porous Si materials are used in LIBs because they accelerate the Li^+ transfer, greater insertion kinetic, and exceptionally improved specific capacity at elevated current density. These 3D porous Si materials used as models and stimulants are traditionally made by the Stöber method [33, 34].

During the manufacture, commercial magnesium (powder form) is used to create pores. The reaction takes place between the commercial magnesium and $HSiCl_3$ in presence of the amine as a catalyst to obtain high-yield porous Si. The final product is obtained after a pyrrole polymerization and heating procedure as shown in Fig.1. The more powerful and costly operative synthetic way may encourage advanced study of the elementary properties of nanoporous Si particles for commercial LIBs.

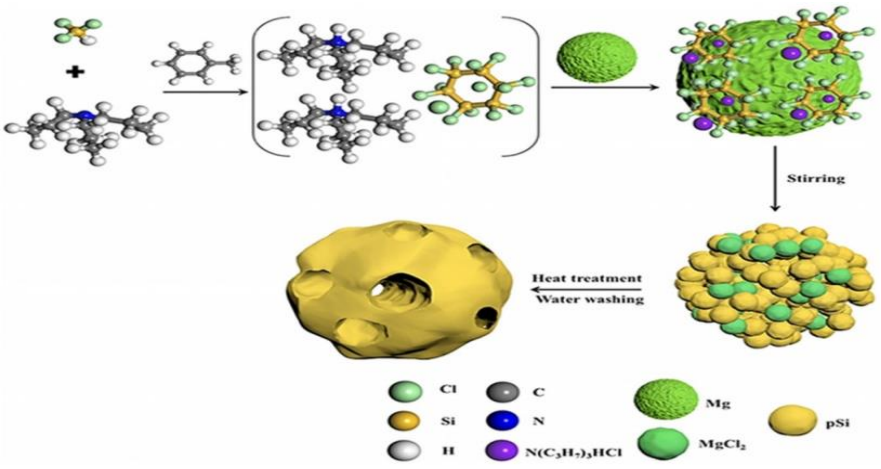

Figure 1. Pattern of the synthetic way to porous Si

2. EXPERIMENTAL

In this section, different materials were used such as silicon powder, proppant, copper, polyethylene oxide (PEO), polyvinyl alcohol (PVA), lithium phosphorous hexafluoride (Li PF_6), ethylene carbonate (EC), polyethylene (separator), lithium sodium vanadium phosphate ($Li_{0.5}Na_{2.5}V_2(PO_4)_3$) as cathode material, aluminum, carbon black slurry, carbon (C), and carbon nanotube (CNT). Two types of cylindrical cells with uniform characteristics were also used: one ICR cell (BYD, ICR18650 -2C) (I1) and five rechargeable cells NCR (Panasonic, 18650-2C) (N2, N3, N4, N5, N6). ICR cell is based on lithium cobalt oxide ($LiCoO_2$) as cathode material, NCR cell used Lithium Nickel Manganese Cobalt Oxide (Li-NMC) as cathode material and both cells used the same Si anode material and PEO + $LiPF_6$ -EC + 10% C as electrolyte. Each cell could charge up to 4.15V±10mV (open circuit voltage) and discharge until the cell reaches a cut voltage of 2.5V±10mV. The experimental system of the multicell LIB was made using a current sensing resistor at 5mΩ (Welwyn Components, OAR-3), electronic load (TEXIO, LW151-151D), and data logger (KEYENCE, NR-500) used for terminal voltage and current measurements. All the materials and chemicals were used as purchased from Sigma-Aldrich Chemicals Pvt. Ltd, India.

Silicon 3D porous anode material is prepared using silicon powder, proppant. Deionized water was used for ultrasonication, acetone, and methanol as a solvent for metal degreasing and copper as anode coating material. As an electrolyte, polyethylene oxide (PEO)/lithium phosphorous hexafluoride (Li PF_6) with ethylene carbonate (EC) composites are used with acetonitrile as solvent. $Li_{0.5}Na_{2.5}V_2(PO_4)_3$ was chosen as cathode material, aluminum, and copper both are used as current collectors where the outer electrode was traditionally prepared using polyvinyl alcohol (PVA) and carbon black slurry.

The silicon 3D porous anode is fabricated by thoroughly mixing silicon powder (mixed with carbon or carbon nanotubes from 0 to 10%), with a particle size of the order of 10 nm to 20 μm with a proppant such as hydrogen peroxide, naphthalene, dichlorobenzene or ammonium bicarbonate with a particle size of from 10nm to 500 nm. The mixing of the two main components must be thorough and is typically a mechanical mixing and ball milling procedure. The mixture (silicon powder and proppant) is then pressed into any nominal form such as a round disc a square disc or a rod, in a press at up to 10,000 psi. at room temperature with thickness > 0.3 mm. The anode can be pressed to a fixed thickness or it can be sliced from a thick rod after final processing. Proppant powders that can be used in this process include hydrogen peroxide, naphthalene, dichlorobenzene, and ammonium bicarbonates but are not limited to these materials. Any (non-reactive with nickel) nanopowder materials that can be evaporated, reduced, and removed under high temperature (25˚C – 400°C) processing can function as proppants in this process. In addition, carbon and or carbon nanotubes may also be appropriate for more open volume and higher electrical conductivity.

The sample when removed from the high-temperature processing furnace is typically smaller in size than that of the initially pressed metal powder/proppant sample. The silicon 3D porous sample is then sliced to the desired thickness and weight. One side of the sample at least is mechanically polished using polishing past then ultrasonically cleaned using deionized water followed by acetone and methanol degreasing. The surface and bulk pore size of the sample is nominally varying around 100 nm to 2 microns. The final step of preparing the silicon 3D porous anode is to coat one side with copper with

thickness 1-10 microns, this process can be done using sputtering, thermal evaporation, or E-beam evaporation techniques. The silicon 3D porous anode is then characterized using SEM, XRD, Raman scattering approaches. After characterization, the prepared anode material is ready to be used in any LIB.

Poly(ethylene oxide)/lithium phosphorous hexafluoride with ethylene carbonate (EC) composites was used as an electrolyte to fabricate electrochemical cells, which significantly improves the capacity of the cell. The cell was manufactured using $Li_{0.5}Na_{2.5}V_2(PO_4)_3$ as a cathode and highly porous silicon material as an anode material. Both aluminum and copper collectors were attached to the outer electrode surface by using 5% PVA mixed with carbon black slurry. The Si| PEO: Li PF_6-EC| $Li_{0.5}Na_{2.5}V_2$ $(PO_4)_3$ electrochemical cell was built up inside a glove box and covered with air-tightened Teflon at ambient temperature. The polymeric solution is prepared by dissolving the 3.5 gm of composite in 10 ml of acetonitrile and it was plunged over the anodic layer separated by porous polyethylene thin films. The thickness of the whole cell is 2.4 mm and was later covered with Teflon though two outlets of copper connections were placed to carry out the electrochemical analysis of the fabricated cell. A schematic diagram of the 3D porous Si-based battery is shown below in Fig. 2. Finally, the LIB cell was electrically tested and the different parameters (open circuit voltage, short circuit current, current density, discharge capacity, power and energy densities) have been determined.

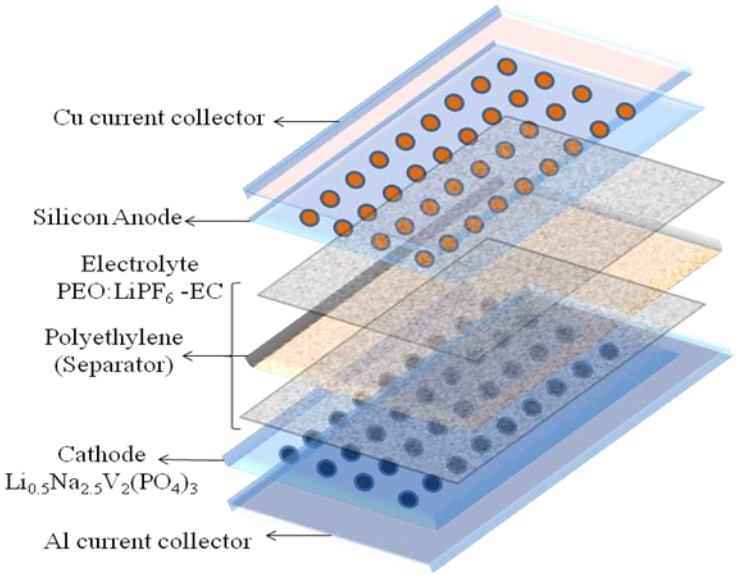

Figure 2. Assembly of Li-ion cell components

3. RESULTS AND DISCUSSION

3.1 SEM characterization of the 3D porous Silicon samples

Fig. 3 shows the SEM pictures of the synthesized 3D porous Si materials for different resolution magnifications. The surface morphology of the prepared samples reveals the existence of 3D interconnected porous microstructures (Fig 3). One can notice that prepared material consists of Si nanosheets forming porous interconnected 3D architectures (Fig. 3a). A relative conventional low magnification SEM picture is observed in Fig 3 b. The lattice image of the high magnification SEM

reveals the presence of Si aggregates that confirms the crystallinity of Si nanosheets. Figure 3 strongly indicates that porous Si particles are unequally dispersed with different sizes. However, the 3D images observed at different scales (× 10,000; × 15,000 and × 60,000 magnifications) reveal that the morphology of pores remains asymmetric. A large surface area and high porosity of Si nanosheets can be beneficial for ion transport. In LIB, the channel of connected porous sites can then shrink the lithium-ion track increasing the migration rate of Li^+ into the Si anode material which enhances the battery performance. In nanomaterials, the energy barrier required for nucleation needs to be smaller due to the large fragment of the Si atoms in high-energy states at the highly metastable surfaces [35–38].

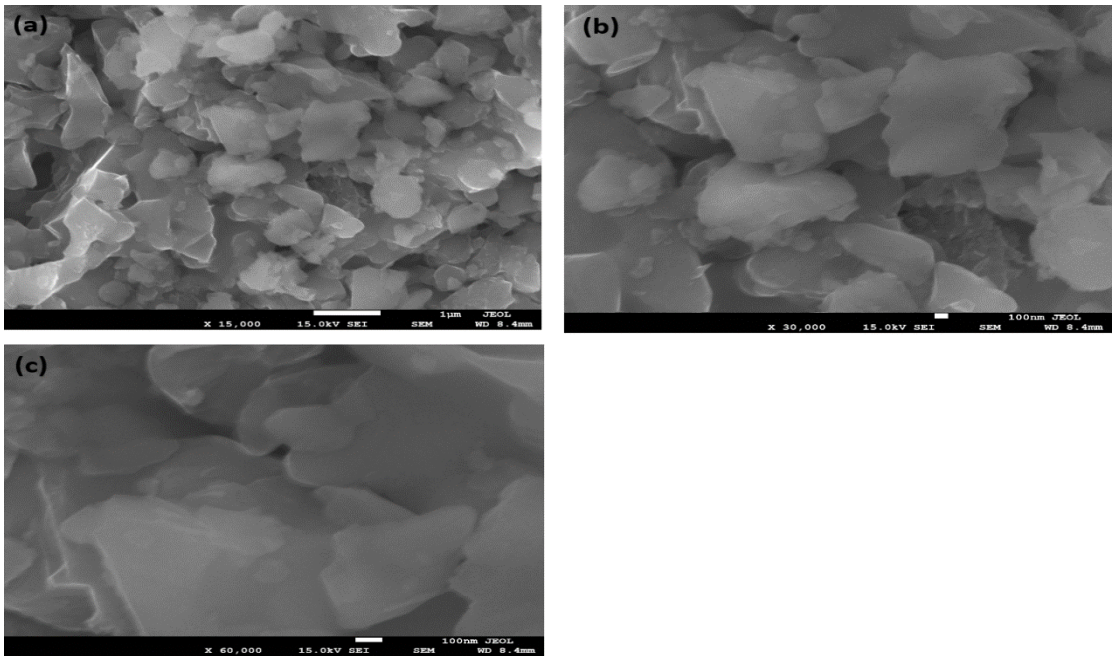

Figure 3. SEM micrographs of 3D porous Si materials for different magnifications. (a) and (b) SEM pictures of low magnification and (c) high magnification.

3.2 X-ray Diffraction

Fig 4. Reveals the XRD pattern of the synthesized porous Si particles. It reveals the appearance of various diffraction planes localized at different positions. The crystalline peaks observed at 28.3,47.2, 56.1, 69 and 76.2° can be referred to (111), (220), (311), (400) and (331) diffraction planes respectively, corresponding to a cubic structure (space group: $Fd\bar{3}m$) (JCPDS: 27-1402) [39]. The XRD pattern also reveals some weak peaks at 35.8, 41.8, and 71.5° which can be assigned to (131), (112), and (431) planes. The broad peak observed at 4° indicates the presence of an amorphous phase in a porous silicon matrix. This indicates the crystalline phase is dominant over the amorphous phase, but the 3D porous Si product still contains an amorphous phase. This confirms the synthesized porous Si is semi-crystalline.

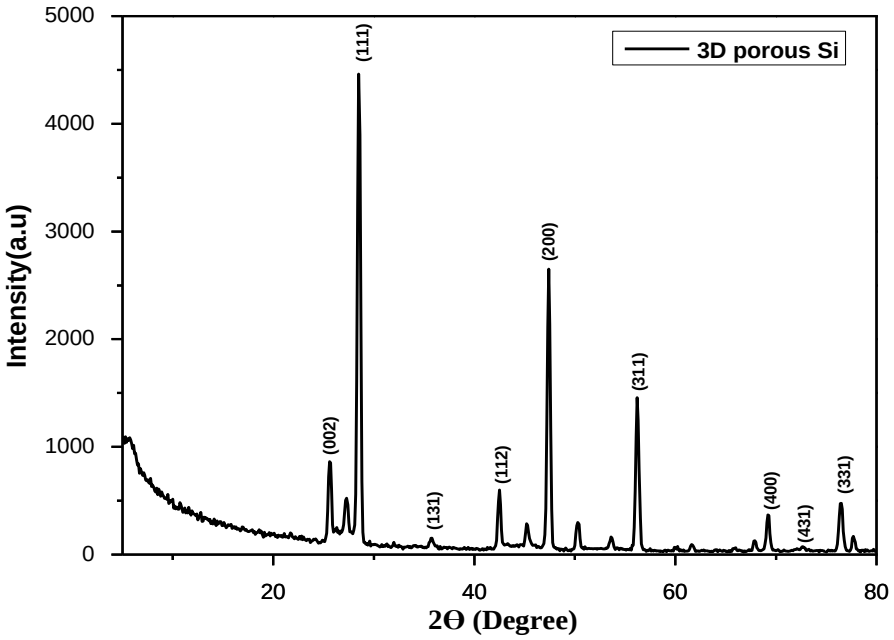

Figure 4. XRD pattern of 3D porous Si particles

3.3 Raman studies of 3D porous silicon

Raman scattering of porous Si material has been investigated. The spectrum indicates three peaks at 300, 508, and 928cm^{-1}as shown in Fig.5.

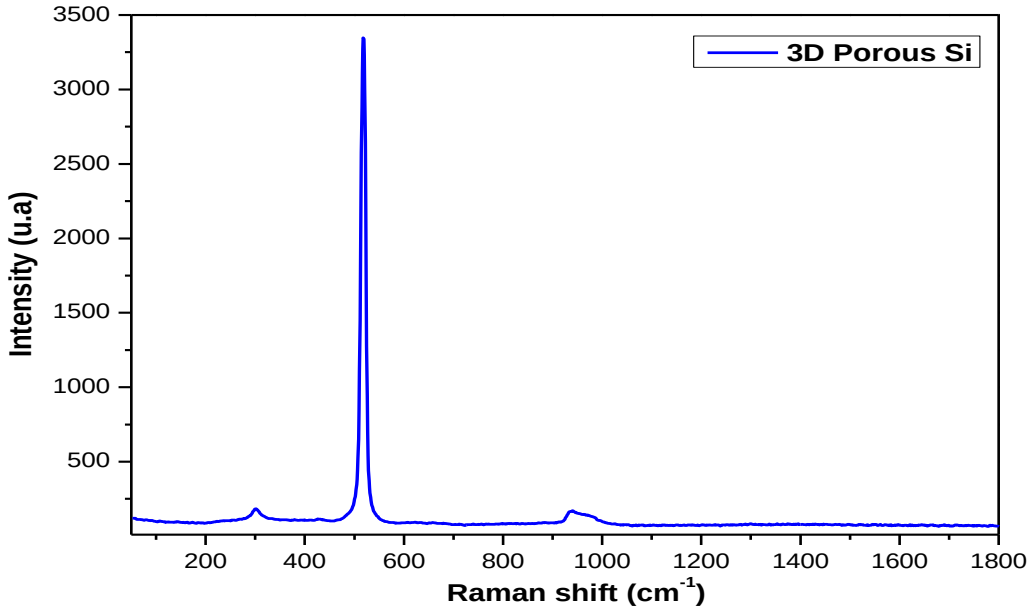

Figure 5. Raman spectrum of porous Si material

These strong peaks reveal the presence of crystallites in the Si sample. Peak position, width, and intensity depend on the porosity of the Si structure as shown in Fig 3. It should be noted the intensity of the Raman peak is proportional to Si density and the length of photon diffusion in the porous Si material [40]. A beam of light reaches the crystalline surface of Si and disperses over Si crystallites and the internal Si atoms will scatter the remaining photons entered in the material [41].

3.4 Electrochemical characterization of the synthesized porous Si

The discharge features of six cells: one ICR cell (I1) and five NCR cells (N2, N3, N4, N5 and N6) cross-connected and discharged to a load of 50kΩ are studied. Fig. 6 shows the association of the cells combined in series connection of I1 || N2 and N3+ N5 || N4 + N6. Each cell was initially charged up to its maximum capacity under the conditions of constant current. However, the discharge capacity (Q) is increased when I1 || N2 (in parallel) and equal to Q_S (I1) + Q_S (N2) but is found to be reduced when they are connected in series. In conclusion, the discharge capacity of the LIB relies on the disposition and the final voltage of every cell [42].

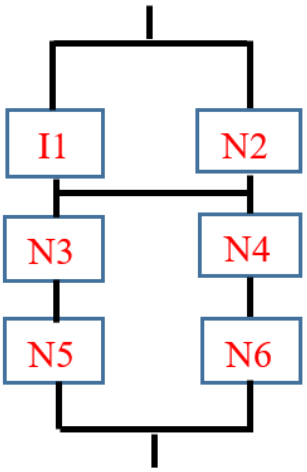

Figure 6. Structure of LIB based on six cells cross coupled.

Discharge characteristics of the fabricated cell: Si| PEO: $LiPF_6$ -EC| (PEO + $LiPF_6$ -EC + 10% of C) at room temperature for a constant load of 100 kΩ (=50 kΩ×2) is shown below in Fig. 7. The voltage of each cell decreases and becomes sable between 75-200 hours after which it sharply goes down. None of the cells reached its cut-off voltage after 300 hours. It should be noted the initial decline in voltage could be due to the activation polarization and/or the formation of a thin film of lithium at the electrode-electrolyte interface. The open-circuit voltage (OCV), short circuit current (SCC), and plateau regions of Li^+: PEO of solid polymer electrolyte cells are tabulated below. It has been found that the silicon introduced Li^+: PEO blended polymer nanocomposite cell showed enhanced electrochemical performances [43-45]. This is highly due to the high surface area of porous silicon combined with a higher ionic conductivity of the selected polymer electrolyte [45] As a conclusion, porous silicon-based

polymer blend electrolyte could be a potential material to promote ion transport [44, 45] in solid-state cells. The cell parameter values are given in table 1.

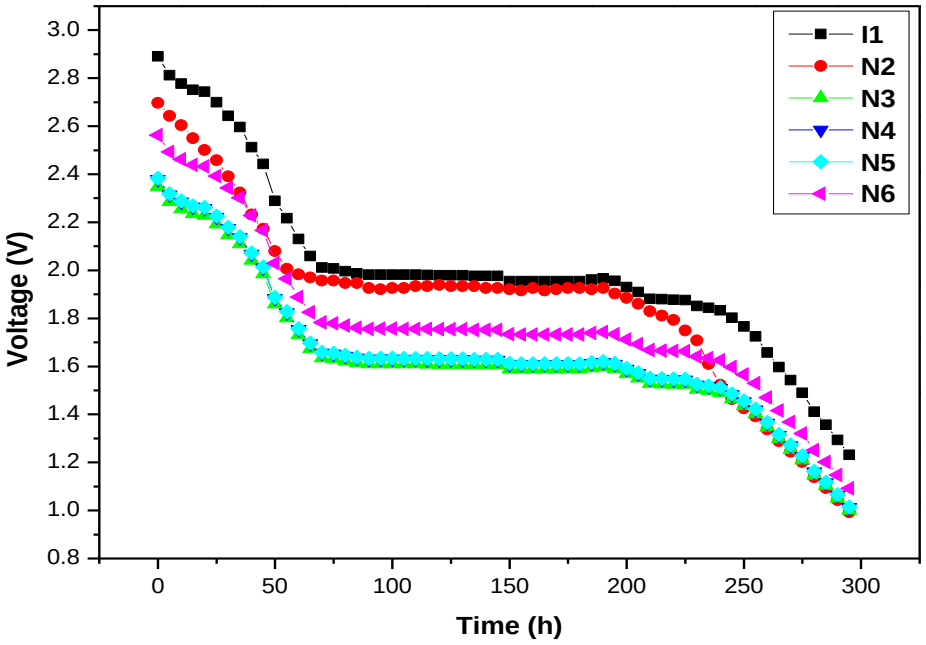

Figure 7. Voltage vs. Time for six cells in in series-parallel connection with cross coupling at ambient temperature at 298 μA cm^{-2} at room temperature.

Table 1. Values of the cell parameters obtained using the prepared 3D porous Si sample as active material in rechargeable LIB

Cell parameters	**Li-Si-Na Battery**
Open circuit voltage (v)	2.61
Short Circuit Current (μA)	242
Cell area (cm^2)	1.161
Cell weight (g)	1.12
Discharge time for plateau region (h)	232
Current density (μA cm^{-2})	298
Power density (Wkg^{-1})	0.74
Energy density (Wh kg^{-1})	387.46
Discharge capacity (μAh^{-1})	0.87

The cyclic capacity of the 3D porous Si has been studied as well as its stability. Fig 8 shows the discharge capacity and efficiency (%) curves of the pure porous Si sample, and its capacity performance. 3D porous Si reveals a gradual decrease in capacity starting from 238.3 to 30 mAh g^{-1} after 100 cycle. This result was compared to that obtained by Y Tang and his co-workers [46] when using novel

composite material $Li_2NaV_2(PO4)_3/C$, the cell exhibited a discharge capacity of 119.1 mAh g^{-1}, of which 93.6% is accumulated nearly 3.7 V vs. Li/Li^+ between 3.0-4.4V at the same 0.1C rate. This demonstrates the electrochemical behavior was influenced by the porosity effect [47,48] of anode material which contributed to enhancing the cell capacity over a lower voltage of 1-2.9V vs Li^+/Li.

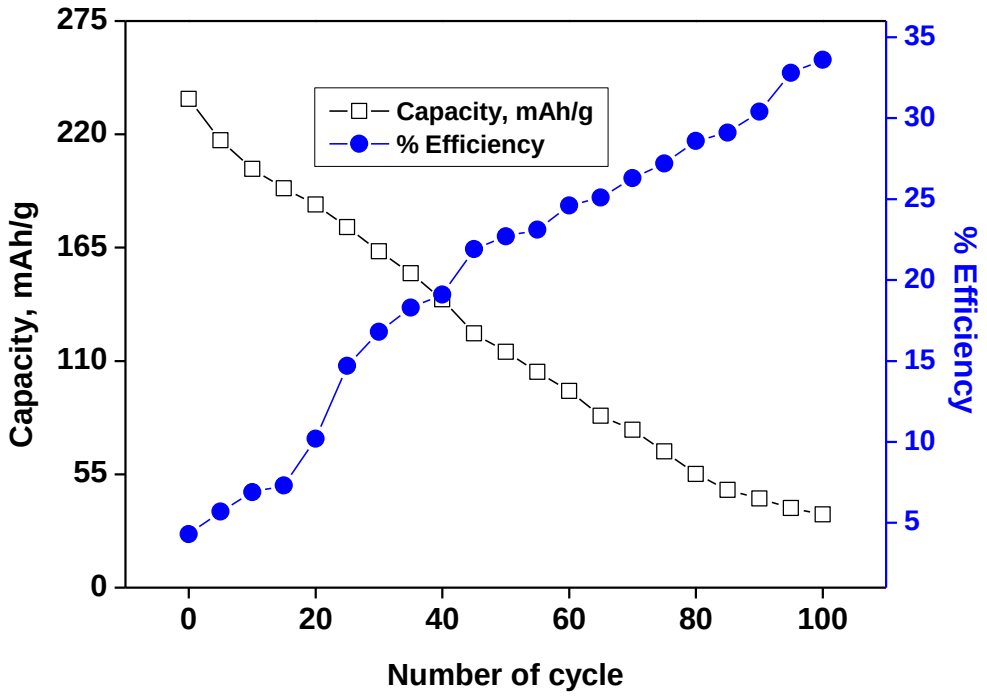

Figure 8. Cyclic performance of the cell at 596 mAg^{-1} for 100 cycles between 1-2.9V vs Li^+/Li for the synthesized Si sample

This capacity decrease is caused by the process of insertion /extraction of Li^+ ions which changed the porous Si volume. However, the coulombic efficiency increases rapidly to 34% after 100cycles. As an alternative to improve this initial value of efficiency, a quantity of SiO2 can be transformed into porous Si material as revealed in Fig. 3 using the magnesiothermic reduction method [48]. This will have a significant impact on the initial coulombic efficiency due to the influence of SiO2 film on the Si nanosheet. The 3D porous structure contributes to reducing the growth of a large volume of Si material, increasing the capacity performance and the coulombic efficiency of the anode material [49-51]. In the synthesis of porous anode materials for LIBs, pore size is a crucial factor that requires much consideration [52, 53] Using nanomaterials is an appropriate way for enhancing the electrochemical performance of LIBs [54].

The loss in capacity loss during the first cycle is caused by the degradation of electrolyte and side reactions occurring irreversibly between the lithium ions and active materials [55]. However, there is no capacity fading up to 50 cycles. While operating, the charge capacity declines from 267.1 and 265.8 mAh g^{-1} and the capacity of retention of 99.5% which is higher than 93.5% obtained by Y Tang [46]

using $Li_2NaV_2(PO4)_3$/C material. However, 22.5 % of the current efficiency was initially released in the battery and the capacity appears to be stable between 40-50 cycles as shown in Fig. 9

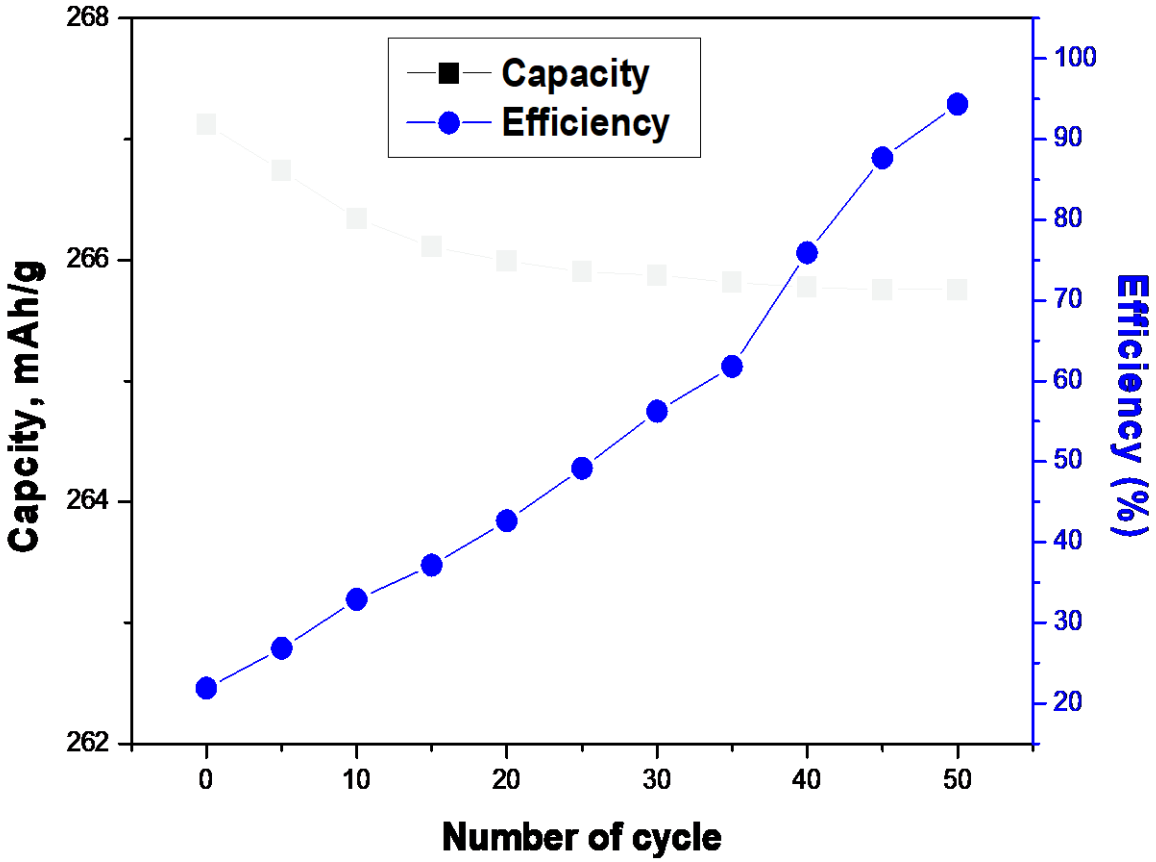

Figure 9. Cyclic stability of the Si material at 298 mA g^{-1} between 1-2.9V vs Li^+/Li for 50cycles

4. CONCLUSION

3D porous Si particles have been synthesized as anode material using silicon powder and proppant for rechargeable LIB via a simple and effective method of sputtering, thermal evaporation. The effect of crystalline shape, porosity, and volume of porous Si have been studied using Raman and the results were confirmed by SEM images. The channel of interconnected porous structures played a great interest in the Li^+ migration and also enhances the capacity performance in the LIB cell. The crystalline phase present in the synthesized 3D porous Si confirmed the structural arrangement of Si crystallites (white particles) and amorphous regions (dark regions) which facilitate the motion of Li-ions throughout the anode material with interconnected pores less than 100 nm. The porosity of bulk Si particles enhanced the volumetric energy density and capacity performance of LIB. The battery delivered a discharge capacity of 267.1 mAh g^{-1} at 298 mA g^{-1}, the coulombic efficiency reached up to 95.5% after 50 cycles and the battery capacity remains stable between 40-50 cycles, with 95.5% of capacity retention.

These results are relatively better than some reported results using $Li_2NaV_2(PO4)_3$ cathode without 3D porous Si anode material. Although the porosity has played a crucial role in performance enhancement, a deep study to comprehend the correlation between the porosity, pore size and material properties is necessary.

ACKNOWLEDGMENTS
Authors NB and ASA would like to acknowledge the financial support towards this research from the Deanship of Scientific Research (DSR), the University of Tabuk, Tabuk, Saudi Arabia, under research Grant No. S-1440-0245.

CONFLICTS OF INTEREST
The authors listed in the manuscript declare that they have no conflict of interest of affiliations or in the subject matter or materials discussed in this manuscript.

References

1. H. Li, X. Huang, L. Chen, Z. Wu and Y. Liang, *Electrochem. Solid-State Lett*., 2 (1999) 547.
2. I.-S. Kim and P. N. Kumta, *J. Power Sources*, 136 (2004) 145.
3. J. Yang, B. F. Wang, K. Wang, Y. Liu, J. Y. Xie and Z. S. Wen, *Electrochem. Solid-State Lett*., 6 (2003), A154.
4. H. Uono, B.-C. Kim, T. Fuse, M. Ue and J. Yamaki, *J. Electrochem. Soc*., 153 (2006), A1708.
5. G. X. Wang, J. H. Ahn, J. Yao, S. Bewlay and H. K. Liu, *Electrochem. Commun.*, 6 (2004) 689.
6. H.-Y. Lee and S.-M. Lee, *Electrochem. Commun*., 6 (2004) 465.
7. N. Dimov, S. Kugino and M. Yoshio, *J. Power Sources*, 136 (2004) 108.
8. S.-H. Ng, J. Wang, D. Wexler, K. Konstantinov, Z.-P. Guo and H.- K. Liu, *Angew. Chem., Int. Ed*., 45(2006) 6896.
9. M. Holzapfel, H. Buqa, W. Scheifele, P. Novak and F.-M. Petrat, *Chem. Commun*., 231(2005), 1566.
10. G. X. Wang, J. Yao and H. K. Liu, *Electrochem. Solid-State Lett*., 7(2004) A250.
11. U. Kasavajjula, C. Wang and A. J. Appleby, *J. Power Sources*, 163 (2007)1003.
12. Y. Kwon, H. Kim, S.-G. Doo and J. Cho, *Chem. Mater*., 19(2007) 982.
13. H. Kim and J. Cho, *J. Electrochem. Soc*., 154 (2007) A462.
14. Y. Kwon, G.-S. Park and J. Cho, *Electrochim. Acta*, 52(2007) 4663.
15. Y. Kwon and J. Cho, *Chem. Commun*., (2008)1109–1112
16. Y.-S. Hu, R. Demir-Cakan, M.-M. Titirici, J.-O. Muller, R. Schlogl, M. Antonietti and J. Maier, *Angew. Chem., Int. Ed*., 47(2008) 1645.
17. H. Ma, F. Cheng, J. Chen, J. Zhao, C. Li, Z. Tao and J. Liang, *Adv. Mater.,* 19(2007) 4067.
18. H. Kim and J. Cho, *Nano Lett*., 7 (2007) 2638.
19. H. Kim and J. Cho, *J. Mater. Chem*., 18 (2008) 771.
20. E. Kim, D. Son, T.-G. Kim, J. Cho, B. Park, K. S. Ryu and S. H. Chang, *Angew. Chem., Int*. Ed., 43(2004) 5987.
21. H. Kim, G.-S. Park, E. Kim, S.-G. Doo and J. Cho, *J. Electrochem. Soc*., 153(2006) A1633.
22. E. Kim, Y. Kim, M. G. Kim and J. Cho, *Electrochem. Solid-State Lett*., 9 (2006) A156
23. H. Wu and Y. Cui, *Nano Today*, 7(2012) 414.
24. M. L. Terranova, S. Orlanducci, E. Tamburri, V. Guglielmotti and M. Rossi, *J. Power Sources*, 246 (2014) 167.
25. J. R. Szczech and S. Jin, *Energy Environ. Sci.,* 4 (2011) 56.
26. B. M. Bang, J. I. Lee, H. Kim, J. Cho and S. Park, *Adv. Energy Mater.*, 2(2012) 878.

27. B. M. Bang, H. Kim, H. K. Song, J. Cho and S. Park, *Energy Environ. Sci*., 4(2011) 5013.
28. S. Sim, P. Oh, S. Park and J. Cho, *Adv. Mater*., 25(2013)4498.
29. J. Cho, Porous Si anode materials for lithium rechargeable batteries. *J. Mater. Chem*., 20(2010) 4009.
30. M. Ge, J. Rong, X. Fang, A. Zhang, Y. Lu and C. Zhou, *Nano Res*., 6 (2013) 174.
31. M. Ge, Y. Lu, P. Ercius, J. Rong, X. Fang, M. Mecklenburg and C. Zhou, *Nano Lett*., 14(2014) 261.
32. Z. Zhang, Z. Li, F. Hao, X. Wang, Q. Li, Y. Qi, R. Fan and L. Yin, *Adv. Funct. Mater*. 24(2013) 2500.
33. H. Kim, B. Han, J. Choo and J. Cho, *Angew. Chem., Int. Ed*., 47(2008) 10151.
34. A. Esmanski and G. A. Ozin, *Adv. Funct. Mater*.,19 (2009),1999.
35. A. Galarneau, H. Cambon, F. D. Renzo, R. Ryoo, M. Choi and F. Fajula, *New J. Chem*., 27 (2003) 73.
36. M.-H. Park, M. G. Kim, J. Choo, K. Kim, J. Kim, S. Ahn, Y. Cui and J. Cho, *Nano Lett*., 9(2009) 3844.
37. J. Graetz, C. C. Ahn, R. Yazami and B. Fultz, *Electrochem. Solid-State Lett.,* 6 (2003), A194.
38. M. J. Gordon, T. Baron, F. Dhalluin, P. Gentile and P. Ferret, *Nano Lett*., 9 (2009) 525-4014.
39. H. Tao, L. Z. Fan, W. L. Song, M. Wu, X. He and X. Qu, *Nanoscale*, 6(2014), 3138.
40. S. Guha, P. Steiner, F. Kozlowski and W. Lang, *J. Porous Mater*. 4(1997) 227–237.
41. R.S. Dariani, and Z. Ahmadi, Optik., 124 (2013) 5353–5356.
42. S. Miyatake, Y. Susuki, T. Hikihara, S. Itoh and K. Tanaka, *J. Power Sources*, 241(2013) 736–743.
43. X. Dong, X. Zheng, Y. Deng, L. Wang, H. Hong and Z. Ju, *J Mater Sci.,*23 (2020) 13023–13035.
44. X. Ding, H. Zhao, D. Liang, and P. He, *Mater. Chem. Phys.,* 267 (2021) 124611.
45. K. Goldshtein, K. Freedman, D. Schneier, L. Burstein, V. Ezersky, E. Peled and D. Golodnitsky*, J. Electrochem. Soc.,* 162 (2015) A1072-A1079.
46. Yuanhao Tang, Chenyun Wang, Jingjing Zhou, Yujing Bi, Yang Liu, Deyu Wang, Siqi Shi and Guobao Li. $Li_2NaV_2(PO4)_3$: A novel composite cathode material with high ratio of rhombohedral phase Journal of Power Sources 227 (2013)199-203.
47. G. Lammel and Ph. Renaudr, *Sens Actuators A Phys.,* 85 (2000) 356–360.
48. Q. Li, L Yin and X. Gao, *RSC Adv.,* 2(2015) 3559.
49. X. Liu, X. Zhu and D. Pan, *R. Soc. open sci*, 5(2018) 172370.
50. W. Luo, X. Chen, Y. Xia, M. Chen, L. Wang, Q. Wang, W. Li and Jianping Yang, *Adv. Energy Mater*, 7 (2017) 1701083.
51. F. Ozanam and M. Rosso, *Mater. Sci. Eng.,* 213(2016) 2-11.
52. K. Zhang, Y. Xia, Zhengdong Yang, R. Fu, C. Shenab and Z. Liu, *RSC Adv.,* 7(2017), 24305–24311.
53. M.S. Al Ja'farawy, D.N. Hikmah, U. Riyadi, A. Purwanto and Hendri Widiyandari, *J. Electron. Mater.* 50, 2021, 6667–6687.
54. M. Ko, S. Chae, and J. Cho, *ChemElectroChem* 2, 2015, 1645.
55. Y. Zhong, T. Shi, Y. Huang, S. Cheng, C. Chen, G. Liao and Z. Tang, *Nanoscale Res. Lett.,* 14 (2019) 85.